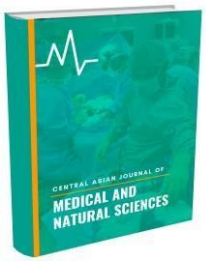

CENTRAL ASIAN JOURNAL OF MEDICAL AND NATURAL SCIENCES
https://cajmns.casjournal.org/index.php/CAJMNS
Volume: 07 Issue: 04 | October 2026 ISSN: 2660-4159

Article

Synthesis, Spectroscopic Characterization, and In Silico Evaluation of Heteroaromatic Chalcone Derivatives at the Colchicine-Binding Site of α/β-Tubulin

Shireen Nadhem Saleh[1]*, Asmaa Adnan Abdulnabi[2], Omeed Muhsin Hassan[3]

1. Department of Pharmaceutical Chemistry, College of Pharmacy, Tikrit University, Salah Al-Din, Iraq
2. Department of Pharmaceutical Chemistry, College of Pharmacy, Al-Nahrain University, Baghdad, Iraq
3. Department of Pharmaceutical Chemistry, College of Pharmacy, University of Kirkuk, Kirkuk, Iraq

* Correspondence: shireen.n.saleh@tu.edu.iq

Abstract: Six heteroaromatic chalcone derivatives (C1–C6) were synthesized by base-catalyzed Claisen–Schmidt condensation and characterized by Fourier-transform infrared (FTIR) and proton nuclear magnetic resonance (^{1}H NMR) spectroscopy. Physicochemical properties, drug-likeness, absorption, distribution, metabolism, and excretion (ADME), toxicity, and predicted tubulin binding were evaluated using SwissADME, ProTox 3.0, and Molecular Operating Environment (MOE) 2019 docking at the colchicine-binding site of α/β-tubulin (Protein Data Bank ID: 4O2B). The docking protocol was validated by re-docking colchicine. The compounds were obtained in 60–80% yields with melting points of 110–196 °C. All derivatives showed zero Lipinski rule-of-five violations and high predicted gastrointestinal absorption. Predicted oral median lethal dose (LD_{50}) values ranged from 800 to 2652 mg/kg. Docking scores ranged from −7.116 to −5.914 kcal/mol. C3 showed the most favorable score (−7.116 kcal/mol) versus re-docked colchicine (−6.992 kcal/mol), with predicted hydrogen bonds to Asn A101 and Lys B254. C3 also had the highest predicted lipophilicity and poorest aqueous solubility, indicating a structure–property trade-off. Experimental tubulin-focused biochemical and cellular studies are required before biological activity can be inferred.

Keywords: Chalcone derivatives, Colchicine-binding site, Molecular docking, ProTox 3.0, SwissADME, Tubulin

Citation: Saleh, S. N, Abdulnabi, A. A & Hassan, O. M. Synthesis, Spectroscopic Characterization, and In Silico Evaluation of Heteroaromatic Chalcone Derivatives at the Colchicine-Binding Site of α/β-Tubulin. Central Asian Journal of Medical and Natural Science 2026, 7(4), 327-339

Received: 13th Jun 2026
Revised: 28th Jul 2026
Accepted: 15th Aug 2026
Published: 03rd Sep 2026

1. Introduction

Cancer remains a major global health burden despite continuing advances in prevention, diagnosis, and treatment. Updated GLOBOCAN estimates for 2024 indicate approximately 20.6 million new cancer cases and 9.8 million cancer deaths worldwide [1]. Therapeutic resistance, tumor heterogeneity, and variable treatment response continue to motivate the search for structurally diverse small molecules directed toward biologically validated targets. Microtubules are particularly important in anticancer drug discovery because they are essential for mitotic-spindle formation, chromosome segregation, intracellular transport, and maintenance of cellular architecture. Their function depends on a tightly regulated balance between tubulin polymerization and depolymerization; pharmacological disruption of this dynamic behavior can impair mitosis and suppress the proliferation of rapidly dividing cells [2,3].

Among the established ligand-binding regions of tubulin, the colchicine-binding site at the α/β-tubulin intradimer interface has attracted sustained medicinal-chemistry interest. The pocket contains both hydrophobic and polar subregions, and ligand

recognition depends on shape complementarity, orientation, hydrogen bonding, and hydrophobic contacts [4,5]. Occupancy of this site can interfere with conformational changes required for productive microtubule assembly. Chalcones are attractive scaffolds for exploring this pocket because their α,β-unsaturated carbonyl linker connects two readily modifiable aromatic or heteroaromatic regions, allowing systematic variation of steric, electronic, and physicochemical properties. Their modular synthesis by Claisen–Schmidt condensation also facilitates the preparation of structurally related analogues [6,7].

Previous studies have reported chalcone-based compounds with antiproliferative and tubulin-directed activity, including substituted chalcones evaluated at the colchicine site [8], thiophene-containing analogues that inhibit tubulin assembly and colchicine binding [9], and chalcones bearing N-heterocyclic motifs [10]. Because a favorable docking score alone does not establish experimental affinity, tubulin inhibition, anticancer efficacy, or safety, computational binding results are most informative when interpreted alongside physicochemical, ADME, and toxicity predictions. Related work published in the Bulletin of the Chemical Society of Ethiopia further supports the use of chalcone chemistry in biologically oriented medicinal-chemistry workflows: chalcone intermediates have been employed to access heterocyclic candidates evaluated for cytotoxic and c-Met kinase activity, while chalcone-derived pyrazolines have been investigated using molecular docking together with biological testing [11,12]. Accordingly, the present study synthesized six structurally related heteroaromatic chalcone derivatives (C1–C6), characterized them by FTIR and ^{1}H NMR spectroscopy, and integrated SwissADME, ProTox 3.0, and molecular-docking results to support comparative structure–property analysis and prioritize compounds for subsequent experimental evaluation. To the best of our knowledge, this exact C1–C6 set has not previously been examined as a unified series at the 4O2B colchicine-binding site within a single workflow integrating experimental spectroscopy, ADME/toxicity prediction, and validated MOE docking. This series-level comparison constitutes the principal novelty of the present work. The overall experimental and computational workflow is summarized in Figure 1.

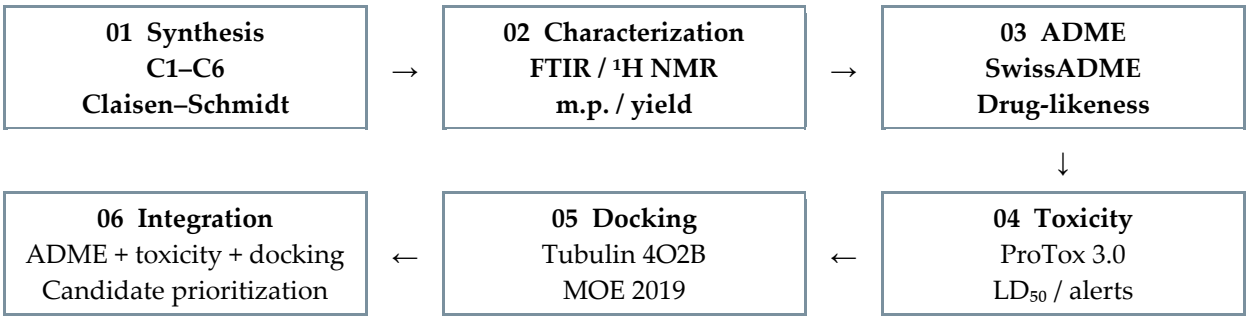

Figure 1. Schematic overview of the experimental and computational workflow used in this study.

2. Materials and Methods

Chemicals and General Experimental Procedure

Reagents and solvents were obtained from Sigma-Aldrich and Merck (Darmstadt, Germany) and used as received, with additional purification where required. The six target chalcone derivatives (C1–C6) were prepared by base-catalyzed Claisen–Schmidt condensation [13]. For each reaction, the appropriate acetyl heteroarene and aldehyde (0.010 mol each) were dissolved in absolute ethanol (15 mL). Sodium hydroxide solution was added slowly, using 40% (w/v) NaOH for C1–C4 and 60% (w/v) NaOH for C5–C6; 1.0 mL was used for C1–C4 and 2.5 mL for C5–C6. The mixtures were stirred at room temperature for 4–6 h, and reaction progress was monitored by thin-layer chromatography (TLC) on silica gel 60 F_{254} plates (Merck KGaA, Darmstadt, Germany) using ethyl acetate/hexane (3:7, v/v) as the mobile phase. Chromatograms were visualized

under UV light at 254 and 366 nm using a CAMAG UV Cabinet 4 (CAMAG, Muttenz, Switzerland). After completion, the products were collected by filtration, washed thoroughly with water to remove residual base, dried, and recrystallized from absolute ethanol. Melting points were determined using a Stuart SMP3 digital melting-point apparatus (Bibby Scientific Ltd., Staffordshire, UK) in the Pharmaceutical Chemistry laboratory, College of Pharmacy, University of Baghdad, Baghdad, Iraq. The general synthetic sequence is presented in Scheme 1.

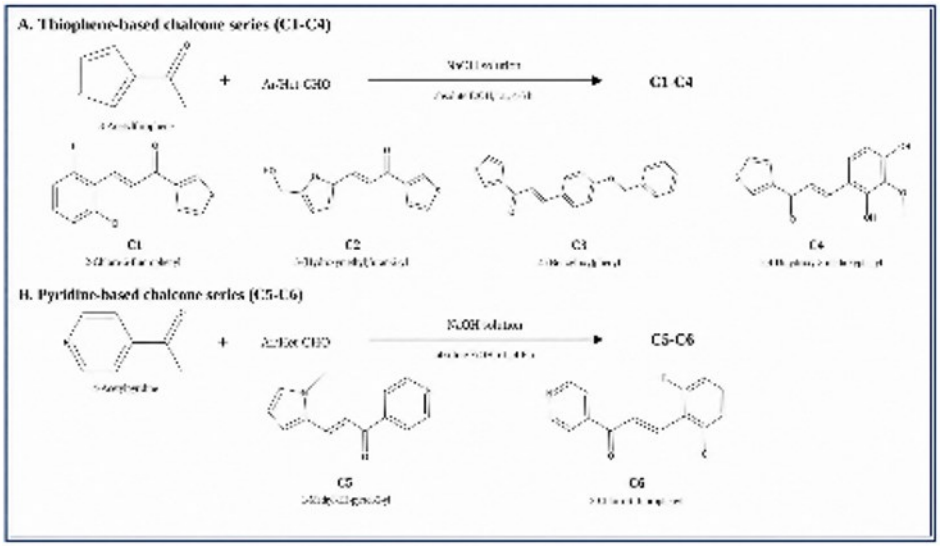

Scheme 1. General synthesis of thiophene- and pyridine-based chalcone derivatives C1–C6 by base-catalyzed Claisen–Schmidt condensation. Reagents and conditions: 40% (w/v) NaOH solution for C1–C4 (1.0 mL) or 60% (w/v) NaOH solution for C5–C6 (2.5 mL); absolute ethanol; room temperature; 4–6 h.

Synthesis of Chalcone Derivatives C1–C6

C1. (E)-3-(2-chloro-6-fluorophenyl)-1-(thiophen-3-yl)prop-2-en-1-one

Prepared from 2-chloro-6-fluorobenzaldehyde and 3-acetylthiophene (0.010 mol each) according to the general procedure, using 1.0 mL of 40% (w/v) NaOH solution. C1 was isolated as a pale-white solid in 80% yield; m.p. 189 °C. Molecular formula: $C_{13}H_8ClFOS$; molecular weight: 266.72 g mol^{-1}.

C2. (E)-3-[5-(hydroxymethyl)furan-2-yl]-1-(thiophen-3-yl)prop-2-en-1-one

Prepared from 5-(hydroxymethyl)furan-2-carbaldehyde and 3-acetylthiophene (0.010 mol each) according to the general procedure, using 1.0 mL of 40% (w/v) NaOH solution. C2 was isolated as a white solid in 75% yield; m.p. 155 °C. Molecular formula: $C_{12}H_{10}O_3S$; molecular weight: 234.27 g mol^{-1}.

C3. (E)-3-[4-(benzyloxy)phenyl]-1-(thiophen-3-yl)prop-2-en-1-one

Prepared from 4-(benzyloxy)benzaldehyde and 3-acetylthiophene (0.010 mol each) according to the general procedure, using 1.0 mL of 40% (w/v) NaOH solution. C3 was isolated as a light-orange solid in 65% yield; m.p. 140 °C. Molecular formula: $C_{20}H_{16}O_2S$; molecular weight: 320.40 g mol^{-1}.

C4. (E)-3-(2,4-dihydroxy-3-methoxyphenyl)-1-(thiophen-3-yl)prop-2-en-1-one

Prepared from 2,4-dihydroxy-3-methoxybenzaldehyde and 3-acetylthiophene (0.010 mol each) according to the general procedure, using 1.0 mL of 40% (w/v) NaOH solution. C4 was isolated as a yellow solid in 70% yield; m.p. 110 °C. Molecular formula: $C_{14}H_{12}O_4S$; molecular weight: 276.31 g mol^{-1}.

C5. (E)-3-(1-methyl-1H-pyrrol-2-yl)-1-(pyridin-4-yl)prop-2-en-1-one

Prepared from 1-methyl-1H-pyrrole-2-carbaldehyde and 4-acetylpyridine (0.010 mol each) according to the general procedure, using 2.5 mL of 60% (w/v) NaOH solution. C5

was isolated as a pale-white solid in 60% yield; m.p. 168 °C. Molecular formula: $C_{13}H_{12}N_2O$; molecular weight: 212.25 g mol^{-1}.

C6. (E)-3-(2-chloro-6-fluorophenyl)-1-(pyridin-4-yl)prop-2-en-1-one

Prepared from 2-chloro-6-fluorobenzaldehyde and 4-acetylpyridine (0.010 mol each) according to the general procedure, using 2.5 mL of 60% (w/v) NaOH solution. C6 was isolated as an orange solid in 77% yield; m.p. 196 °C. Molecular formula: $C_{14}H_9ClFNO$; molecular weight: 261.68 g mol^{-1}.

Spectroscopic Characterization

Fourier-Transform Infrared Spectroscopy

FTIR spectra were recorded to assess the principal functional groups of the synthesized derivatives using an IRXross ATR instrument (Shimadzu Corporation, Kyoto, Japan) at the Department of Chemistry, College of Education, University of Samarra, Iraq. The analysis focused on absorptions associated with the conjugated carbonyl system and substituent-dependent aromatic, heteroaromatic, hydroxyl, and ether functionalities. Compound-specific bands are summarized in the Results and Discussion section.

Proton Nuclear Magnetic Resonance Spectroscopy

^{1}H NMR spectra were acquired at 400.13 MHz on a Bruker AVANCE NEO spectrometer (Bruker BioSpin GmbH, Rheinstetten, Germany) at the Department of Chemistry, College of Education for Women, University of Basrah, Iraq, using DMSO-d_6 as solvent. Chemical shifts are reported as δ values in parts per million (ppm). Spectral interpretation was based on the experimentally observed resonances. Coupling constants were reported only for signals whose splitting patterns were sufficiently resolved; partially overlapped regions were retained as composite observed regions without speculative peak-by-peak assignment.

Physicochemical, Drug-Likeness, and ADME Prediction

The physicochemical and predicted pharmacokinetic properties of C1–C6 were evaluated using SwissADME [14]. The calculated descriptors included molecular weight, topological polar surface area (TPSA), consensus lipophilicity (LogP), ESOL-predicted aqueous solubility, gastrointestinal absorption, blood–brain barrier permeability, P-glycoprotein substrate status, Lipinski rule-of-five compliance, bioavailability score, and medicinal-chemistry alerts, including PAINS and Brenk filters. These outputs were interpreted as comparative in silico descriptors rather than experimentally measured pharmacokinetic parameters.

In Silico Toxicity Prediction

Predicted toxicity profiles were assessed using ProTox 3.0 [15]. The comparative output included the predicted median lethal dose (LD_{50}), acute toxicity class, hepatotoxicity, neurotoxicity, nephrotoxicity, respiratory toxicity, cardiotoxicity, carcinogenicity, immunotoxicity, mutagenicity, and cytotoxicity endpoints. Model confidence and prediction-accuracy information were considered qualitatively when interpreting binary endpoint calls; near-threshold classifications were not over-interpreted. These values were used as model-based screening descriptors for comparison within the series and were not treated as experimental evidence of compound safety or toxicity.

Molecular Docking Studies

Molecular docking was performed at the colchicine-binding site of the α/β-tubulin heterodimer using the tubulin–colchicine crystal structure (PDB ID: 4O2B) obtained from the RCSB Protein Data Bank [16]. The structure was determined by X-ray diffraction at 2.30 Å resolution [16,17]. Docking calculations were carried out with MOE 2019 [18]. Water molecules and non-essential heteroatoms were removed, missing hydrogen atoms were added, and partial charges were assigned using the MMFF94x force field as implemented in MOE [18,19]. Protonation states were assigned at pH 7.4 using Protonate3D [20], and the prepared protein was energy-minimized to an RMS gradient of

0.05 kcal mol^{-1} Å^{-1}. Residue labels in the binding-site analysis correspond to α-tubulin chain A and β-tubulin chain B.

The docking site was defined as a 10 Å sphere centered on the co-crystallized colchicine. Ligand placement used the Triangle Matcher method with London dG scoring, followed by GBVI/WSA dG rescoring. The protocol was validated by re-docking colchicine; the top-ranked pose reproduced the crystallographic orientation with an RMSD of approximately 1.0 Å. Compounds C1–C6 were then docked under the same protocol. Docking scores and predicted hydrogen-bonding, carbon–hydrogen, π-mediated, fluorine-associated, sulfur-associated, and hydrophobic contacts were recorded for comparative interpretation. The docking scores are used only for within-protocol ranking and are not treated as experimental binding free energies.

3. Results

Synthesis and Spectroscopic Characterization

All six heteroaromatic chalcone derivatives (C1–C6) were isolated as solids in yields of 60–80%, with melting points ranging from 110 to 196 °C. The IRXross ATR spectra contained bands consistent with the expected conjugated chalcone framework and substituent-dependent functional groups. The principal conjugated carbonyl-region absorptions occurred between 1639 and 1686 cm^{-1}. C3 additionally showed a band at 1709 cm^{-1}; because the proposed structure contains a single carbonyl group, this additional feature was not used as evidence for a second carbonyl functionality. Hydroxyl-containing derivatives showed higher-frequency absorptions, including 3402 cm^{-1} for C2 and a broad 3418–3233 cm^{-1} region for C4. Selected diagnostic bands for each compound are summarized in Table 1.

The ^{1}H NMR spectra showed aromatic, heteroaromatic, olefinic, and substituent-specific resonances. Where the olefinic signals were sufficiently resolved, large vicinal coupling constants (approximately 15.2–16.7 Hz) were observed, supporting a trans relationship across the α,β-unsaturated double bond and therefore the assigned E configuration for those resolved signals. In C2, the olefinic resonances at δ 7.534–7.496 and 7.399–7.360 ppm showed J ≈ 15.4 and 15.4 Hz, respectively, while the hydroxymethyl substituent was represented by resonances at δ 5.443–5.415 and 4.502–4.488 ppm. In C5, two resolved olefinic doublets at δ 7.785–7.747 and 7.498–7.460 ppm (J ≈ 15.2 Hz for each), together with the N-methyl resonance at δ 3.776 ppm, supported the assigned enone geometry and N-methylpyrrole substituent. C3 additionally showed the expected benzylic OCH_2 resonance at approximately δ 5.19 ppm. For C4, the selected spectrum showed an aromatic/olefinic region at δ 8.28–6.89 ppm and an OMe-region resonance at δ 3.80–3.78 ppm. A downfield resonance at δ 9.305 ppm (br s, 1H) was assigned to a phenolic OH proton. Because the aromatic/olefinic signals of C4 were substantially overlapped, the δ 8.28–6.89 ppm region was retained as a composite observed region rather than subjected to speculative proton-by-proton assignment. Selected physical and spectroscopic data are summarized in Table 1.

Table 1. Selected physical and spectroscopic data for chalcone derivatives C1–C6.

Compound	Yield (%)	m.p. (°C)	Formula / MW (g mol^{-1})	FTIR, νmax (cm^{-1})	Selected ^{1}H NMR data (400.13 MHz, DMSO-d_6), δ (ppm), multiplicity, J
C1	80	189	$C_{13}H_8ClFOS$ 266.72	3086; 1651; 1593; 1562; 1504; 1223	8.725 (s, 1H); 7.945–7.807 (m, ca. 2H); 7.766–7.725 (d, J ≈ 16.7 Hz, 1H); 7.712–7.694 (m, 1H); 7.633–7.450 (m, ca. 2H); 7.405–7.357 (m, ca. 1H)

Compound	Yield (%)	m.p. (°C)	Formula / MW (g mol⁻¹)	FTIR, νmax (cm⁻¹)	Selected ¹H NMR data (400.13 MHz, DMSO-d_6), δ (ppm), multiplicity, J
C2	75	155	$C_{12}H_{10}O_3S$ 234.27	3402; 1643; 1585; 1501; 1285; 1177	8.696–8.693 (d, J ≈ 1.3 Hz, 1H); 7.686–7.666 (m, 1H); 7.618–7.606 (d, J ≈ 4.8 Hz, 1H); 7.534–7.496 (d, J ≈ 15.4 Hz, 1H); 7.399–7.360 (d, J ≈ 15.4 Hz, 1H); 7.032–7.024 (d, J ≈ 3.2 Hz, 1H); 6.516–6.509 (d, J ≈ 3.2 Hz, 1H); 5.443–5.415 (t, J ≈ 5.8 Hz, ca. 1H); 4.502–4.488 (d, J ≈ 5.7 Hz, ca. 2H)
C3	65	140	$C_{20}H_{16}O_2S$ 320.40	3090; 1709; 1647; 1605; 1535; 1250	8.788 (s, ca. 1H); 7.855–7.834 (d, J ≈ 8.6 Hz, ca. 2H); 7.756–7.329 (m, aromatic/olefinic H); 7.121–7.100 (d, J ≈ 8.6 Hz, ca. 2H); 5.190 (s, ca. 2H)
C4	70	110	$C_{14}H_{12}O_4S$ 276.31	3418–3233 (br); 1639; 1578; 1547; 1493; 1285	9.305 (br s, 1H, OH; supporting downfield trace); 8.28–6.89 (m, aromatic/olefinic H); 3.80–3.78 (OMe region)
C5	60	168	$C_{13}H_{12}N_2O$ 212.25	1686; 1651; 1570; 1474; 1273	8.815–8.800 (d, J ≈ 5.8 Hz); 7.939–7.925 (d, J ≈ 5.9 Hz); 7.785–7.747 (d, J ≈ 15.2 Hz); 7.498–7.460 (d, J ≈ 15.2 Hz); 7.146–7.119 (m); 6.932–6.917 (d, J ≈ 5.9 Hz); 6.223–6.209 (app t, J ≈ 2.9 Hz); 3.776 (s, ca. 3H)
C6	77	196	$C_{14}H_9ClFNO$ 261.68	3075; 1647; 1612; 1597; 1574; 1481; 1296	8.857–8.845 (d, J ≈ 4.6 Hz); 8.140–7.999 (m); 7.817–7.803 (d, J ≈ 5.9 Hz); 7.741–7.080 (m)

Note. br = broad; app = apparent; m = multiplet. Coupling constants are reported only for resolved line patterns in the ¹H NMR spectra (400.13 MHz).

Partially overlapped regions are reported directly as composite observed regions without speculative deconvolution; the table lists selected resonances assigned to the target structures rather than every minor signal visible in the full spectra. Minor non-integrated resonances were not used for structural assignment. FTIR values are selected bands from the IRXross ATR spectra and are rounded to the nearest cm⁻¹. Complete original FTIR and ¹H NMR spectra for C1–C6 are provided in the Supplementary Information.

Physicochemical Properties, Drug-Likeness, and ADME Profile

Selected physicochemical, solubility, and drug-likeness descriptors for C1–C6 are summarized in Table 2. Molecular weights ranged from 212.25 to 320.40 g mol⁻¹. All six compounds showed zero Lipinski rule-of-five violations, a predicted bioavailability score

of 0.55, and no PAINS alerts in the reported output. Each compound also returned one Brenk alert (michael_acceptor_1), consistent with the conjugated α,β-unsaturated carbonyl motif intrinsic to the chalcone scaffold; this was treated as a scaffold-level reactivity flag rather than evidence of nonspecific biological activity. Consensus LogP values ranged from 1.67 for C5 to 4.82 for C3, while TPSA values ranged from 29.96 Å² for C6 to 95.00 Å² for C4. C2 and C5 had the least negative ESOL LogS values and therefore the comparatively more favorable predicted aqueous solubility, whereas C3 had the most negative predicted LogS value (−5.03).

All six derivatives were predicted to have high gastrointestinal absorption and none was predicted to be a P-glycoprotein substrate. C1, C3, C5, and C6 were predicted to cross the blood–brain barrier, whereas C2 and C4 were not. The latter two compounds also had the highest TPSA values in the series, consistent with their greater predicted polarity. These absorption, blood–brain barrier, and P-glycoprotein classifications are visualized in Figure 2 and should not be interpreted as measured human pharmacokinetic behavior.

Table 2. Selected physicochemical, solubility, and drug-likeness descriptors of C1–C6 predicted by SwissADME.

Compound	MW	TPSA (Å²)	Consensus LogP	ESOL LogS	Lipinski violations	Bioavailability score
C1	266.72	45.31	4.49	−4.36	0	0.55
C2	234.27	78.68	2.11	−2.51	0	0.55
C3	320.40	54.54	4.82	−5.03	0	0.55
C4	276.31	95.00	2.55	−3.37	0	0.55
C5	212.25	34.89	1.67	−2.35	0	0.55
C6	261.68	29.96	3.66	−3.87	0	0.55

Note. MW = molecular weight; TPSA = topological polar surface area; LogS = ESOL-predicted aqueous solubility. All values are computational predictions and not experimentally measured pharmacokinetic parameters.

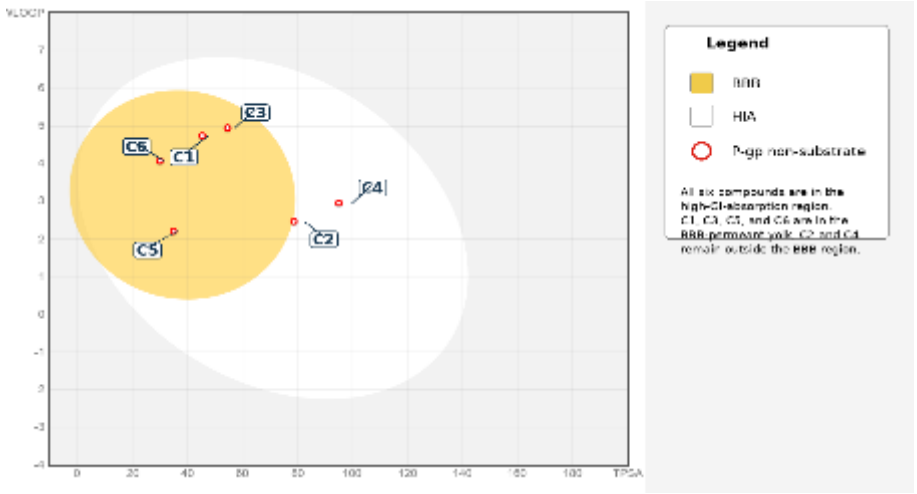

Figure 2. BOILED-Egg model illustrating the predicted gastrointestinal absorption and blood–brain barrier permeation of C1–C6.

The BOILED-Egg plot provides a complementary visualization of the SwissADME absorption predictions. In the reported model, all six compounds fell within the white region associated with high gastrointestinal absorption, whereas only C1, C3, C5, and C6 were located in the yellow yolk associated with predicted blood–brain barrier permeation; C2 and C4 remained outside the BBB-permeant region. The plot is intended as a screening

representation and does not constitute experimental evidence of systemic or central nervous system exposure. The corresponding model is shown in Figure 2.

Predicted Toxicity Profile

The predicted toxicity profiles of C1–C6 were assessed using ProTox 3.0 and are summarized in Table 3. Predicted oral LD_{50} values ranged from 800 to 2652 mg/kg. C1, C2, C3, C5, and C6 were assigned to acute toxicity class 4, whereas C4 was assigned to class 5 and had the highest predicted LD_{50} (2652 mg/kg). C2 had the lowest predicted LD_{50} (800 mg/kg) [15].

None of the six compounds was classified as active for hepatotoxicity, cardiotoxicity, carcinogenicity, or cytotoxicity in the reported ProTox 3.0 output. The ProTox cytotoxicity endpoint is a model-based toxicity classification and should not be interpreted as an experimental cancer-cell antiproliferative assay. Other predicted alerts varied across the series: C1 and C6 were classified as active for neurotoxicity and immunotoxicity; C2 for nephrotoxicity, respiratory toxicity, and mutagenicity; C3 for immunotoxicity; C4 for nephrotoxicity and immunotoxicity; and C5 for neurotoxicity, respiratory toxicity, and immunotoxicity. Prediction confidence varied across compounds and endpoints, and the binary labels were therefore interpreted as screening flags rather than definitive toxicological outcomes.

Table 3. Predicted acute oral toxicity and selected toxicity endpoints of C1–C6.

Compound	LD_{50} (mg/kg)	Acute toxicity class	Hepato-toxicity	Neuro-toxicity	Nephro-toxicity	Respiratory toxicity	Cardio-toxicity	Carcino-genicity	Immuno-toxicity	Muta-genicity	Cyto-toxicity
C1	1800	4	Inactive	Active	Inactive	Inactive	Inactive	Inactive	Active	Inactive	Inactive
C2	800	4	Inactive	Inactive	Active	Active	Inactive	Inactive	Inactive	Active	Inactive
C3	1000	4	Inactive	Inactive	Inactive	Inactive	Inactive	Inactive	Active	Inactive	Inactive
C4	2652	5	Inactive	Inactive	Active	Inactive	Inactive	Inactive	Active	Inactive	Inactive
C5	1000	4	Inactive	Active	Inactive	Active	Inactive	Inactive	Active	Inactive	Inactive
C6	2000	4	Inactive	Active	Inactive	Inactive	Inactive	Inactive	Active	Inactive	Inactive

Note. ProTox 3.0 outputs are model-based screening predictions. 'Active' and 'Inactive' denote the corresponding prediction class and do not represent experimentally confirmed toxicological outcomes. Model confidence and prediction accuracy varied across compounds and endpoints; near-threshold classifications should therefore be interpreted cautiously.

The toxicity predictions did not produce a single uniformly favorable profile. C4 had the least severe predicted acute toxicity classification in the series (class 5), whereas C2 combined the lowest predicted LD_{50} with the largest number of selected endpoint alerts. Accordingly, the toxicity output is most informative when considered together with the docking and ADME results rather than used as a stand-alone ranking criterion.

Molecular Docking and Binding Interactions

Docking was performed at the colchicine-binding site of α/β-tubulin (PDB ID: 4O2B), a structurally characterized pocket occupied by colchicine and other microtubule-destabilizing ligands [5,16,17]. Re-docking of colchicine reproduced its crystallographic

orientation with an RMSD of approximately 1.0 Å, supporting use of the selected protocol for comparative pose generation. The docking scores ranged from −5.914 to −7.116 kcal/mol. C3 gave the most favorable score among the synthesized compounds (−7.116 kcal/mol), followed by C1 (−6.301), C6 (−6.163), C2 (−6.027), C4 (−5.916), and C5 (−5.914); the re-docked colchicine reference scored −6.992 kcal/mol. Because these values are scoring-function outputs, the small numerical differences should be interpreted as comparative ranking within this protocol rather than as measured binding affinities. Docking scores and selected interaction patterns are summarized in Table 4, with representative interaction diagrams shown in Figures 3A and 3B.

The predicted interaction patterns differed across the series. C3 formed conventional hydrogen bonds with Asn A101 and Lys B254 (2.16 Å each), together with a π-donor hydrogen-bond contact involving Asn B249 and a software-identified π–sulfur contact with Tyr A224. C1 showed software-identified sulfur-associated and π-mediated contacts involving Val B238, Cys B241, and Lys B254 in addition to hydrophobic interactions, whereas C2 was dominated by hydrophobic contacts. C4 formed a conventional hydrogen bond with Asn A101 and a carbon–hydrogen contact with Ser A178. C5 showed mainly carbon–hydrogen and hydrophobic contacts. C6 formed conventional hydrogen bonds with Lys B254 and Asn A101, together with a fluorine-associated noncovalent contact identified in the docking interaction map. These interaction maps help rationalize the docked poses but do not by themselves establish inhibitory activity.

Table 4. MOE docking scores, selected protein–ligand contacts, and chemical structures of C1–C6 and colchicine at the tubulin colchicine-binding site (PDB ID: 4O2B).

No.	ID	Docking score (kcal/mol)	Selected binding residues / interaction type	Structure
1	C1	-6.301	Software-identified sulfur-associated contact: Val B238 (3.30 Å); π–sigma: Cys B241 (2.72 Å); amide–π stacked contact involving Lys B254. Hydrophobic contacts: Leu B242, Ala A180, Ala B250, Leu B248, Leu B255, Lys B352.	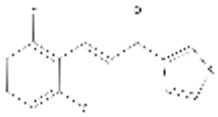
2	C2	-6.027	Predominantly hydrophobic contacts: Leu B248 (5.14 Å), Leu B255 (4.04 Å), Ala B250 (3.71 Å), Lys B352 (3.95 Å), Met B259 (4.89 Å), Ala B316 (5.18 Å).	
3	**C3**	**-7.116**	**Conventional H-bonds: Asn A101 (2.16 Å), Lys B254 (2.16 Å); π-donor H-bond: Asn B249; software-identified π–sulfur contact: Tyr A224. Hydrophobic contacts: Ala B250, Ala A180, Leu B248, Lys B352, Ala B354, Ala B316.**	

No.	ID	Docking score (kcal/mol)	Selected binding residues / interaction type	Structure
4	C4	-5.916	Conventional H-bond: Asn A101 (2.18 Å); carbon–hydrogen contact: Ser A178 (2.84 Å). Hydrophobic contacts: Ala B316, Leu B255, Cys B241, Ala B250, Leu B248, Ala A180.	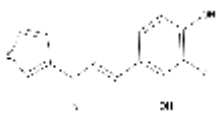
5	C5	-5.914	Carbon–hydrogen contacts: Asn A101 (2.68 Å), Asn B350 (2.71, 2.77 Å), Ala A180 (2.46 Å). Hydrophobic contacts: Ala B250, Lys B254, Leu B248, Lys B352, Met B259, Val A181, Ala B316.	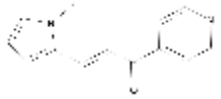
6	C6	-6.163	Conventional H-bonds: Lys B254 (2.63 Å), Asn A101 (2.38 Å); carbon–hydrogen contacts: Ala A180 (2.51 Å), Val B315 (2.58 Å); fluorine-associated noncovalent contact. Hydrophobic contacts: Leu B248, Ala B250, Lys B352, Met B259, Val A181, Ala B316.	
-	Colchicine	-6.992	Carbon–hydrogen contacts: Asn A101 (2.87, 2.99 Å), Asp B251 (2.40, 2.62 Å), Val B238 (2.50, 2.67 Å). Hydrophobic contacts: Ala B250, Leu B242, Cys B241, Ile B318, Ala B316, Ala B354, Ala A180.	

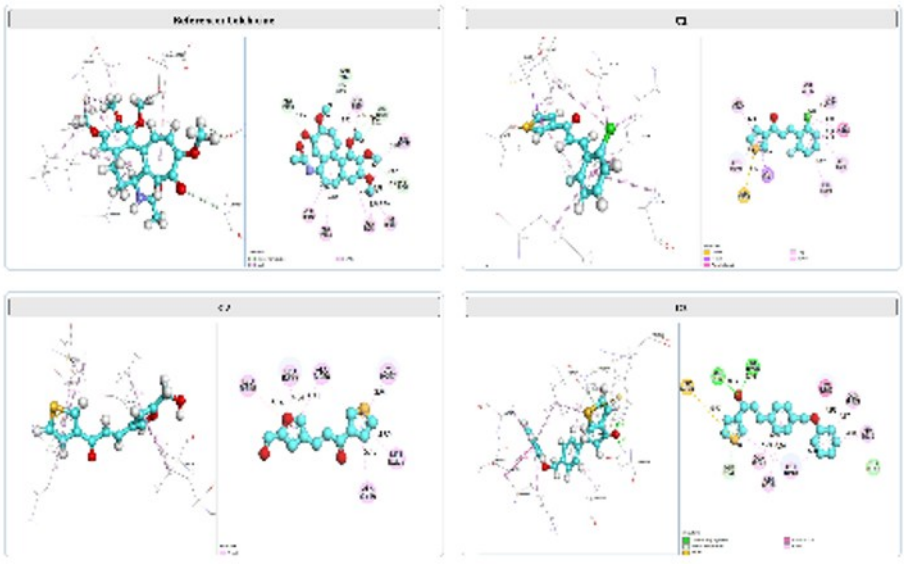

Figure 3A. Representative 3D and 2D interaction diagrams for the re-docked colchicine reference and compounds C1–C3 at the tubulin colchicine-binding site (PDB ID: 4O2B).

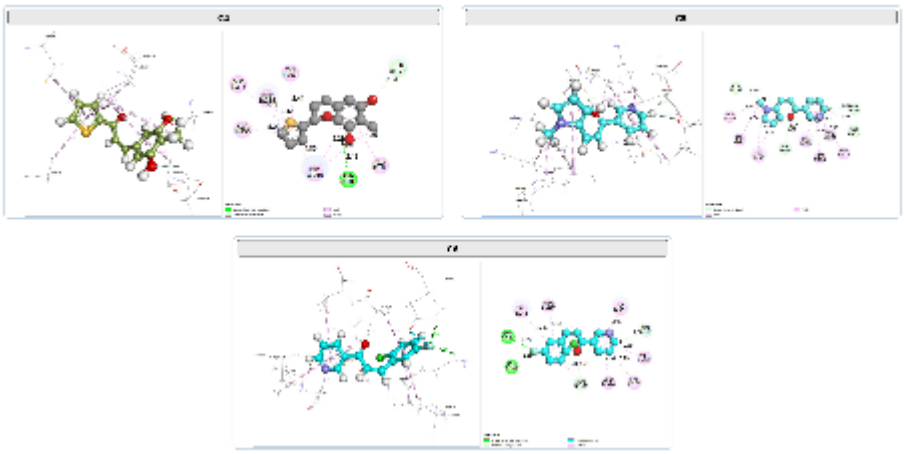

Figure 3B. Representative 3D and 2D interaction diagrams for compounds C4–C6 at the tubulin colchicine-binding site (PDB ID: 4O2B).

C3 emerged as the strongest docking candidate in the series, with a score of −7.116 kcal/mol, compared with −6.992 kcal/mol for the re-docked colchicine reference. The numerical difference is small and should not be interpreted as evidence that C3 binds more strongly than colchicine; rather, it places C3 at the top of the present series under the same scoring protocol. Its predicted pose combined two conventional hydrogen bonds with Asn A101 and Lys B254 with an extended set of hydrophobic contacts, providing a more balanced interaction pattern than was observed for the lower-ranked analogues.

A structural rationale for the ranking can be drawn from the way C3 occupies the colchicine-binding pocket. The benzyloxy-substituted aromatic region increases the hydrophobic surface of the molecule, while the docked pose places C3 in contact with Ala B250, Leu B248, Ala B316, Lys B352, and other residues that form part of the predominantly hydrophobic environment of the colchicine site [5]. This behavior is consistent with the general medicinal-chemistry profile of colchicine-site ligands, for which productive hydrophobic occupancy is important alongside appropriately positioned polar contacts. Previous studies have also shown that chalcone derivatives and thiophene-containing chalcone analogues can display tubulin-directed and antiproliferative activity [8,9]. Those reports support the relevance of the scaffold class, although they do not establish biological activity for C3 or any other member of the present series.

The comparison between C1 and C6 is particularly useful because both compounds contain the same 2-chloro-6-fluorophenyl region but differ in the heteroaromatic ring attached to the carbonyl group. C1, bearing a thiophene ring, produced a slightly more favorable score than the pyridine-containing C6 (−6.301 versus −6.163 kcal/mol). In contrast, C6 formed two conventional hydrogen bonds in its predicted pose. This contrast shows that hydrogen-bond count alone did not determine the docking rank; the overall fit of the ligand, hydrophobic packing, and the combined geometry of multiple contacts contributed to the calculated score.

The lower-ranked compounds further illustrate this balance. C4 formed a conventional hydrogen bond with Asn A101, yet its score remained among the least favorable in the series, whereas C2 was stabilized mainly by hydrophobic contacts without achieving a comparable score to C3. C5, the smallest and least lipophilic member of the series, also gave the weakest docking score. Taken together, these observations suggest that, within this limited set, productive occupation of the hydrophobic region together with well-positioned polar contacts was more favorable than either polarity or hydrogen bonding alone. Because this interpretation is derived from a docking model, it

should be tested experimentally rather than treated as a definitive structure–activity relationship.

4. Discussion

Integrated Structure-Property Interpretation

The combined analysis highlights a clear structure–property trade-off rather than a single uniformly superior compound. C3 ranked first in docking, but the same structural features that favor extensive hydrophobic contact with the tubulin pocket are accompanied by the highest predicted lipophilicity in the series (Consensus LogP 4.82) and the least favorable ESOL-predicted solubility (LogS −5.03). Its docking advantage therefore has to be weighed against a less favorable predicted aqueous-solubility profile. C4 represents the opposite end of this balance: it had the highest polarity, was not predicted to cross the blood–brain barrier, and showed the least severe acute toxicity class, but its docking score was among the weakest. These contrasting profiles are important because they show that improving one calculated property did not automatically improve the others. All six compounds also shared the same Brenk michael-acceptor alert arising from the chalcone enone, so this scaffold-level flag does not differentiate the series but remains relevant for subsequent experimental assessment. On the present evidence, C3 is the most reasonable first compound for tubulin-focused follow-up, while C1 and C6 provide useful secondary candidates with different interaction patterns. Experimental tubulin-polymerization and cancer-cell assays will be required to determine whether the computational ranking translates into biological activity.

5. Conclusion

Six heteroaromatic chalcone derivatives (C1–C6) were synthesized, characterized by FTIR and ^{1}H NMR spectroscopy, and evaluated using a combined in silico workflow. The series showed consistent predicted oral drug-likeness but clear differences in lipophilicity, aqueous solubility, toxicity alerts, and docking behavior. Under the applied MOE protocol, C3 gave the most favorable docking score at the tubulin colchicine-binding site, while C1 and C6 provided secondary docking profiles of interest. C3 also showed the highest predicted lipophilicity and the poorest ESOL-predicted solubility, illustrating that docking score alone is insufficient for candidate selection. C3 is therefore prioritized for follow-up within this computational series. Because no biochemical or cellular efficacy experiments were performed, tubulin-polymerization and antiproliferative assays are required before biological activity can be inferred.

Acknowledgements

The authors received no financial, material, or technical support for this study.

Data Availability

The data supporting the findings of this study are available from the corresponding author upon reasonable request.

Conflict of Interest

The authors declare no conflict of interest.

Funding

This research received no external funding or specific grant.

REFERENCES

[1] H. Sung, A. M. Filho, M. Laversanne, J. Ferlay, R. L. Siegel, I. Soerjomataram, A. Jemal, and F. Bray, "Global cancer statistics 2024: GLOBOCAN estimates of incidence and mortality worldwide for 34 cancers in 186 countries," *CA Cancer J. Clin.*, vol. 76, Art. no. e70090, 2026, doi: 10.3322/caac.70090.

[2] H. C. Assunção, P. M. A. Silva, H. Bousbaa, and H. Cidade, "Recent advances in microtubule targeting agents for cancer therapy," *Molecules*, vol. 30, Art. no. 3314, 2025, doi: 10.3390/molecules30163314.

[3] E. Pasquier and M. Kavallaris, "Microtubules: A dynamic target in cancer therapy," *IUBMB Life*, vol. 60, pp. 165–170, 2008, doi: 10.1002/iub.25.

[4] E. C. McLoughlin and N. M. O'Boyle, "Colchicine-binding site inhibitors from chemistry to clinic: A review," *Pharmaceuticals*, vol. 13, Art. no. 8, 2020, doi: 10.3390/ph13010008.
[5] J. Wang, D. D. Miller, and W. Li, "Molecular interactions at the colchicine binding site in tubulin: An X-ray crystallography perspective," *Drug Discov. Today*, vol. 27, pp. 759–776, 2022, doi: 10.1016/j.drudis.2021.12.001.
[6] C. Zhuang, W. Zhang, C. Sheng, W. Zhang, C. Xing, and Z. Miao, "Chalcone: A privileged structure in medicinal chemistry," *Chem. Rev.*, vol. 117, pp. 7762–7810, 2017, doi: 10.1021/acs.chemrev.7b00020.
[7] N. A. A. A. Elkanzi, H. Hrichi, R. A. Alolayan, W. Derafa, F. M. Zahou, and R. B. Bakr, "Synthesis of chalcone derivatives and their biological activities: A review," *ACS Omega*, vol. 7, pp. 27769–27786, 2022, doi: 10.1021/acsomega.2c01779.
[8] H. Zhang, J. J. Liu, J. Sun, X. H. Yang, T. T. Zhao, X. Lu, H. B. Gong, and H. L. Zhu, "Design, synthesis and biological evaluation of novel chalcone derivatives as antitubulin agents," *Bioorg. Med. Chem.*, vol. 20, pp. 3212–3218, 2012, doi: 10.1016/j.bmc.2012.03.055.
[9] R. Romagnoli, P. G. Baraldi, M. D. Carrion, C. Lopez Cara, O. Cruz-Lopez, D. Preti, M. Tolomeo, S. Grimaudo, A. Di Cristina, N. Zonta, J. Balzarini, A. Brancale, T. Sarkar, and E. Hamel, "Design, synthesis, and biological evaluation of thiophene analogues of chalcones," *Bioorg. Med. Chem.*, vol. 16, pp. 5367–5376, 2008, doi: 10.1016/j.bmc.2008.04.026.
[10] K. Mezgebe, Y. Melaku, and E. Mulugeta, "Synthesis and pharmacological activities of chalcone and its derivatives bearing N-heterocyclic scaffolds: A review," *ACS Omega*, vol. 8, pp. 19194–19211, 2023, doi: 10.1021/acsomega.3c01035.
[11] R. M. Mohareb, A. A. Mohamed, and R. A. Ibrahim, "Uses of chalcone acetophenone to synthesis heterocyclic compounds with cytotoxic and c-Met kinase activities," *Bull. Chem. Soc. Ethiop.*, vol. 36, pp. 149–172, 2022, doi: 10.4314/bcse.v36i1.13.
[12] K. M. Qadir, H. Y. Hussein, M. Y. Aziz, M. M. Ayoob, M. K. Samad, A. J. Hussien, N. G. Ahmed, and F. E. Hawaiz, "Synthesis, molecular docking study and antibacterial activity of new pyrazoline derivatives," *Bull. Chem. Soc. Ethiop.*, vol. 39, pp. 955–966, 2025, doi: 10.4314/bcse.v39i5.11.
[13] M. A. Shalaby, S. A. Rizk, and A. M. Fahim, "Synthesis, reactions and application of chalcones: A systematic review," *Org. Biomol. Chem.*, vol. 21, pp. 5317–5346, 2023, doi: 10.1039/D3OB00792H.
[14] A. Daina, O. Michielin, and V. Zoete, "SwissADME: A free web tool to evaluate pharmacokinetics, drug-likeness and medicinal chemistry friendliness of small molecules," *Sci. Rep.*, vol. 7, Art. no. 42717, 2017, doi: 10.1038/srep42717.
[15] P. Banerjee, E. Kemmler, M. Dunkel, and R. Preissner, "ProTox 3.0: A webserver for the prediction of toxicity of chemicals," *Nucleic Acids Res.*, vol. 52, pp. W513–W520, 2024, doi: 10.1093/nar/gkae303.
[16] RCSB Protein Data Bank, "4O2B: Tubulin-colchicine complex," RCSB PDB, 2014, doi: 10.2210/pdb4O2B/pdb.
[17] A. E. Prota, F. Danel, F. Bachmann, K. Bargsten, R. M. Buey, J. Pohlmann, S. Reinelt, H. Lane, and M. O. Steinmetz, "The novel microtubule-destabilizing drug BAL27862 binds to the colchicine site of tubulin with distinct effects on microtubule organization," *J. Mol. Biol.*, vol. 426, pp. 1848–1860, 2014, doi: 10.1016/j.jmb.2014.02.005.
[18] Chemical Computing Group ULC, *Molecular Operating Environment (MOE)*, version 2019.01. Montreal, QC, Canada: Chemical Computing Group ULC, 2019.
[19] T. A. Halgren, "Merck molecular force field. I. Basis, form, scope, parameterization, and performance of MMFF94," *J. Comput. Chem.*, vol. 17, pp. 490–519, 1996, doi: 10.1002/(SICI)1096-987X(199604)17:5/6<490::AID-JCC1>3.0.CO;2-P.
[20] P. Labute, "Protonate3D: Assignment of ionization states and hydrogen coordinates to macromolecular structures," *Proteins*, vol. 75, pp. 187–205, 2009, doi: 10.1002/prot.22234.